THERMO-ELASTOHYDRODYNAMIC ANALYSIS OF PISTON CONNECTING-ROD BIG END JOURNAL BEARING LUBRICATION SYSTEM

Huey Jiuan Low[1], William Woei Fong Chong[2]*

[1]School of Mechanical Engineering, Faculty of Engineering
Universiti Teknologi Malaysia
81310 UTM Johor Bahru, Johor, Malaysia

[2]Automotive Development Centre (ADC)
Faculty of Engineering
Universiti Teknologi Malaysia (UTM)
81310 UTM Johor Bahru, Johor, Malaysia

Article history
Received
9 September 2020
Received in revised form
9 December 2020
Accepted
9 December 2020
Published
15 December 2020

*Corresponding author
lowhueyjiuan@gmail.com

ABSTRACT

The existence of friction could be both detrimental and beneficial. On the one hand, friction prevents slipping on a moving vehicle but on the other hand, friction induces by the engine tends to reduce the power. In an engine, friction can be reduced by introducing an effective lubrication system.Hence, the aim of the present study is to derive a thermo-elastohydrodynamic mathematical model to predict lubricant film formation properties along the piston connecting-rod big end journal bearing lubrication system. A thermo - elastohydrodynamic mathematical model is implemented by integrating an Energy equation with2-D Reynolds equation to solve the lubricant film formation along the piston connecting-rod big end journal bearing. It is used to deduce the tribological properties of the lubricant, namely contact pressure and film profile. Under isothermal condition with increasing lubricant viscosity, both pressure hydrodynamic and film thickness increase. Similar results are demonstrated when there is an increase in the velocity or applied normal load. Under thermal condition, the viscous heating generated during the engine operation tends to increase the temperature, leading to the reduction of lubricant viscosity and film thickness. The mathematical model is simulated and compared with the literature data obtained. However, the simulated results do not correlate well with the literature data although the mathematical model is capable in predicting film thickness in the similar range. This could be due to the underestimation on the effect of transient squeeze film effect in this model.

KEYWORDS

Thermo-elastohydrodynamic; 2-D Reynolds Equation; 2-D Energy Equation; Contact Pressure; Film Profile.

NOMENCLATURE

c_p	Specific heat of lubricant (J/(kg.K))
h	Lubricant film (m)
k_t	Thermal conductivity of lubricant (W/(m.K))
p	Contact pressure (Pa)
u	Sliding velocity in x-direction (m/s)
u_{av}	Average sliding velocity (ms)
x	Domain x in the sliding direction (m)
y	Domain y perpendicular to the sliding direction (m)
z	Domain z perpendicular to xy plane (m)
F	Residual term for numerical solution (-)
H	Non-dimensional lubricant film (-)
J	Jacobian matrix (-)
P	Non-dimensional contact pressure (-)
T	Lubricant temperature (K)
U	Non-dimensional sliding velocity in x-direction (-)
W_x	Load in x-direction (N)
W_y	Load in y-direction (N)
$W_{resultant}$	Resultant load (N)
X	Non-dimensional domain x in the sliding direction (-)
Y	Non-dimensional domain y perpendicular to the sliding direction (-)
δ	Surface deflection (m)
η	Lubricant viscosity (Pa.s)
$\bar{\eta}$	Non-dimensional lubricant viscosity (-)
γ	Coefficient of thermal expansion of lubricant (-)
ρ	Lubricant density (kg/m^3)
$\bar{\rho}$	Non-dimensional lubricant density (-)

1.0 INTRODUCTION

In general, friction refers to the force that acts in the opposite to resist sliding or rolling motion between solid surfaces, material elements as well as fluid layers confined between opposing surfaces. Friction is considered as a necessary evil because it could be both vital and detriment to our daily life. Without friction, basic activities such as standing and walking on a surface, could be impossible. Contradictorily, the presence of friction generates a resistive force that causes energy loss in mechanical machines, especially in automotive industries.

In the year of 2009, it was found that 208,000 million litres of fuel (gasoline and diesel) were used to overcome the friction in passenger cars around the world [1]. Out of the 208,000 million litres of fuel, almost one-third of the fuel energy was lost to the friction generated in engine system. Friction generated by the bearing systems in typical passenger cars was found to take up approximately 30% of fuel energy required by the engine system [1,2]. Out of all the bearings in an engine, piston connecting-rod big end journal bearing has been found to greatly contribute to the total bearing losses by the engine system.

During the operating of internal combustion engine, the frictional behaviour is not only dependent on the dynamic loading, but also influenced by the thermal effect towards the lubricant. Viscosity of the lubricant drops along with the increment in the fluid film temperature. At the same time, lubricant film strength, which refers to the function of viscosity that, relies on both pressure and temperature, will be affected. Consequently, the fluid film thickness and the ability of the contact to carry load might be reduced due to the drop in lubricant viscosity at higher operating temperatures [3,4].

Analysis on elastohydrodynamic problem is considered to be difficult due to its complexity because viscosity changes exponentially with both pressure and temperature. There are several studies conducted on elastohydrodynamic problems as to show the importance of considering thermal effects in the bearing analysis.Under the study of isothermal and thermal analysis, Karthikeyan et al. [3] proposed to simultaneously solve Reynolds equation, energy equation along

with lubricant rheology. In addition, based on Kim and Kim [5], cavitation phenomenon, elastic deformation, bearing surface thermal distortion and viscosity variation due to the temperature are all vital in the analysis of connecting-rod bearings. El-Butch [6] presented that both elastic and thermal deformations significantly influence the hydrodynamic pressure and oil film thickness. Whist Cheng andSternlight [7] improvised on existing elastohydrodynamic solutions by introducing a better temperature analysis that ensures better prediction of film thickness, pressure and temperature by solving Reynolds coupled with energy numerically. As for Kim et al. [8], they proposed a new numerical formulation by considering the lubricant as a Newtonian fluid along with a two-dimensional energy equation which the changing temperature throughout the film is taken to be a quadratic profile.

Energy saving and environmental friendly features have become more emphasized throughout the years in machine design. Gao et al. [9] presented a water-lubricated plain journal bearing, however, water exhibits a lower viscosity than oil, which contributes to lower load carrying capacity. On the other hand, Zhang et al. [10] found that gas compressibility tends to reduce the change of pressure in gas-lubricated bearings, which leads to a smaller load capacity than oil-lubricated bearings. It is particularly difficult to produce the most appropriate choice of effective water-lubricated and oil-lubricated journal bearings.

All the above mentioned studies conducted show significant relationship between thermal effects with the bearing lubrication system. It is essential to account for the thermal effects towards the frictional behaviour of the piston connecting-rod big end journal bearing so as to allow for further enhancement of the performance of internal combustion engine. Hence, the aim of the present study is to derive a thermo-elastohydrodynamic mathematical model to predict lubricant film formation properties along the piston connecting-rod big end journal bearing lubrication system.

2.0 METHODOLOGY

For the present study, the properties of the simulated piston connecting rod big end journal bearing are adopted from reference [11,12].The tribological properties, namely contact pressure and film profile, are investigated at four sets of operating conditions as highlighted in Figure 1. It is to note that locations A and B focus on the change of velocity (Figure 1(a)) while locations C and D emphasize on the effect of applied normal load (Figure 1(b)).

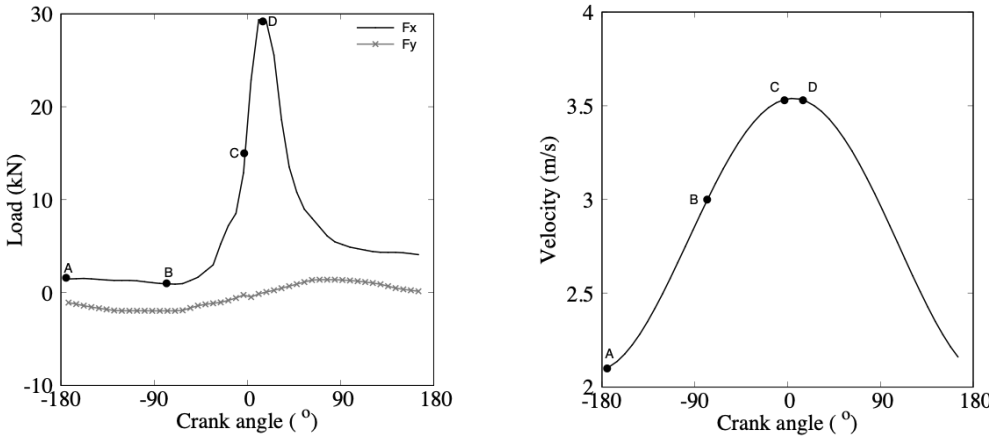

(a) Applied normal load on the connecting-rod big end journal bearing

(b) Velocity on the connecting-rod big end journal bearing

Figure 1 (a) and (b): Simulated contact conditions for piston connecting rod big end journal bearing

2.12-Dimensional Reynolds Equation

To apply the Reynolds equation for the piston connecting-rod big end journal bearing lubrication, several assumptions should be considered to simplify the 2-D Reynolds equation. The assumptions

are, 1) Laminar flow, 2) Incompressible flow, 3) Newtonian fluid, 4) Squeeze term is negligible, 5) Entrainment velocity in y-direction is negligible and 6) Curvature effects are negligible. By referring to the assumptions above, the pressure distribution in the lubrication film for the piston connecting-rod big end journal bearing can be determined using the simplified 2-D Reynolds equation with Reynolds boundary condition:

$$\frac{\partial}{\partial x}\left(\frac{\rho h^3}{\eta}\cdot\frac{\partial p}{\partial x}\right)+\frac{\partial}{\partial y}\left(\frac{\rho h^3}{\eta}\cdot\frac{\partial p}{\partial y}\right) = 12\left\{\frac{\partial(\rho h u)}{\partial x}\right\} \tag{1}$$

2.2 Derivation of Numerical Mathematical Model

By applying all the dimensionless parameters as given in reference [3,4,13], the dimensionless form of 2-D Reynolds equation is as shown below:

$$\frac{\partial}{\partial X}\left[\frac{\bar{\rho}H^3}{\bar{\eta}}\cdot\frac{\partial P}{\partial X}\right]+\frac{\partial}{\partial Y}\left[\frac{\bar{\rho}H^3}{\bar{\eta}}\cdot\frac{\partial P}{\partial Y}\right] = \psi\cdot\frac{\partial}{\partial X}[\bar{\rho}HU] \tag{2}$$

where $\psi=\frac{12u_{av}\eta_0 R_x^2}{P_h b^3}$

The 2-D Reynolds in Equation 2 is solved numerically through finite difference approximation as explained in reference [3]. All the three terms in that equation are expanded separately into nodal vector (i,j) form by applying central difference method for left hand side terms, whilst central difference and backwards difference method for the right hand side terms.

$$\begin{aligned}\frac{\partial}{\partial X}\left[\frac{\bar{\rho}H^3}{\bar{\eta}}\cdot\frac{\partial P}{\partial X}\right] = \frac{1}{2\Delta X^2}\Bigg\{&\left[\left(\frac{\bar{\rho}H^3}{\bar{\eta}}\right)_{i+1,j}+\left(\frac{\bar{\rho}H^3}{\bar{\eta}}\right)_{i,j}\right]P_{i+1,j}\\ &-\left[\left(\frac{\bar{\rho}H^3}{\bar{\eta}}\right)_{i+1,j}+2\left(\frac{\bar{\rho}H^3}{\bar{\eta}}\right)_{i,j}+\left(\frac{\bar{\rho}H^3}{\bar{\eta}}\right)_{i-1,j}\right]P_{i,j}\\ &+\left[\left(\frac{\bar{\rho}H^3}{\bar{\eta}}\right)_{i,j}+\left(\frac{\bar{\rho}H^3}{\bar{\eta}}\right)_{i-1,j}\right]P_{i-1,j}\Bigg\}\\ &= A_{i,j}\end{aligned} \tag{3}$$

$$\begin{aligned}\frac{\partial}{\partial Y}\left[\frac{\bar{\rho}H^3}{\bar{\eta}}\cdot\frac{\partial P}{\partial Y}\right] = \frac{1}{2\Delta Y^2}\Bigg\{&\left[\left(\frac{\bar{\rho}H^3}{\bar{\eta}}\right)_{i,j+1}+\left(\frac{\bar{\rho}H^3}{\bar{\eta}}\right)_{i,j}\right]P_{i,j+1}\\ &-\left[\left(\frac{\bar{\rho}H^3}{\bar{\eta}}\right)_{i,j+1}+2\left(\frac{\bar{\rho}H^3}{\bar{\eta}}\right)_{i,j}+\left(\frac{\bar{\rho}H^3}{\bar{\eta}}\right)_{i,j-1}\right]P_{i,j}\\ &+\left[\left(\frac{\bar{\rho}H^3}{\bar{\eta}}\right)_{i,j}+\left(\frac{\bar{\rho}H^3}{\bar{\eta}}\right)_{i,j-1}\right]P_{i-1,j}\Bigg\}\\ &= B_{i,j}\end{aligned} \tag{4}$$

$$\frac{\partial}{\partial X}[\bar{\rho}HU] = \frac{(\bar{\rho}H^3U)_{i,j} - (\bar{\rho}H^3U)_{i-1,j}}{\Delta X} = C_{i,j} \tag{5}$$

By replacing Equation (3-5) into Equation (2), the simplified representation of the equations is given as follow:

$$A_{i,j} + B_{i,j} = \psi C_{i,j} \tag{6}$$

The modified Newton-Raphson method is then applied to solve for the Equation (6) as given in references [3,4]. The residual term, $F_{i,j}$ is arranged to form the equation below:

$$F_{i,j} = A_{i,j} + B_{i,j} - \psi \cdot C_{i,j} \tag{7}$$

Then, Equations (3-5) are substituted back into Equation 7, which forms:

$$\begin{aligned} F_{i,j} = \frac{1}{2\Delta X^2}\Bigg\{&\left[\left(\frac{\bar{\rho}H^3}{\bar{\eta}}\right)_{i+1,j} + \left(\frac{\bar{\rho}H^3}{\bar{\eta}}\right)_{i,j}\right]P_{i+1,j} \\ &- \left[\left(\frac{\bar{\rho}H^3}{\bar{\eta}}\right)_{i+1,j} + 2\left(\frac{\bar{\rho}H^3}{\bar{\eta}}\right)_{i,j} + \left(\frac{\bar{\rho}H^3}{\bar{\eta}}\right)_{i-1,j}\right]P_{i,j} \\ &+ \left[\left(\frac{\bar{\rho}H^3}{\bar{\eta}}\right)_{i,j} + \left(\frac{\bar{\rho}H^3}{\bar{\eta}}\right)_{i-1,j}\right]P_{i-1,j}\Bigg\} \\ &+ \frac{1}{2\Delta Y^2}\Bigg\{\left[\left(\frac{\bar{\rho}H^3}{\bar{\eta}}\right)_{i,j+1} + \left(\frac{\bar{\rho}H^3}{\bar{\eta}}\right)_{i,j}\right]P_{i,j+1} \\ &- \left[\left(\frac{\bar{\rho}H^3}{\bar{\eta}}\right)_{i,j+1} + 2\left(\frac{\bar{\rho}H^3}{\bar{\eta}}\right)_{i,j} + \left(\frac{\bar{\rho}H^3}{\bar{\eta}}\right)_{i,j-1}\right]P_{i,j} \\ &+ \left[\left(\frac{\bar{\rho}H^3}{\bar{\eta}}\right)_{i,j} + \left(\frac{\bar{\rho}H^3}{\bar{\eta}}\right)_{i,j-1}\right]P_{i-1,j}\Bigg\} - \psi \\ &\cdot\left[\frac{(\bar{\rho}H^3U)_{i,j} - (\bar{\rho}H^3U)_{i-1,j}}{\Delta X}\right] \end{aligned} \tag{8}$$

The Taylor expansion series is then executed to turn Equation (8) into Equation (9) as shown below:

$$\bar{F}_{i,j} = F_{i,j} + \frac{\partial F_{i,j}}{\partial P_{i+1,j}}\Delta P_{i+1,j} + \frac{\partial F_{i,j}}{\partial P_{i-1,j}}\Delta P_{i-1,j} + \frac{\partial F_{i,j}}{\partial P_{i,j}}\Delta P_{i,j} + \frac{\partial F_{i,j}}{\partial P_{i,j+1}}\Delta P_{i,j+1} + \frac{\partial F_{i,j}}{\partial P_{i,j-1}}\Delta P_{i,j-1} \tag{9}$$

where $\Delta P_{i,j} = \bar{P}_{i,j} - P_{i,j}$. By assuming the residual term in the Taylor expansion series approaches zero so as to obtain an approximated solution, where $\bar{F}_{i,j} \approx 0$. Then, the equation is rearranged in terms of the change in pressure, $\Delta P_{i,j}$ as follow:

$$\Delta P_{i,j} = \frac{-F_{i,j} - J_1 \Delta P_{i+1,j} - J_2 \Delta P_{i-1,j} - J_4 \Delta P_{i,j+1} - J_5 \Delta P_{i,j-1}}{J_3} \tag{10}$$

The Jacobian terms, J_1, J_2, J_3, J_4 and J_5 stated in Equation (10) are the partial differential of the residual term with respect of their nodal points. Hence, an example of the Jacobian term, J_1 for elastohydrodynamic condition can be derived as below:

$$J_1 = \frac{\partial F_{i,j}}{\partial P_{i+1,j}}$$

$$\begin{aligned} J_1 = \frac{1}{2\Delta X^2}\Bigg\{ & \left[\left(\frac{\bar{\rho}H^3}{\bar{\eta}}\right)_{i+1,j} + \left(\frac{\bar{\rho}H^3}{\bar{\eta}}\right)_{i,j}\right] P_{i+1,j} - \left[\left(\frac{\bar{\rho}H^3}{\bar{\eta}}\right)_{i+1,j} + 2\left(\frac{\bar{\rho}H^3}{\bar{\eta}}\right)_{i,j} + \left(\frac{\bar{\rho}H^3}{\bar{\eta}}\right)_{i-1,j}\right] P_{i,j} \\ & + \left[\left(\frac{\bar{\rho}H^3}{\bar{\eta}}\right)_{i,j} + \left(\frac{\bar{\rho}H^3}{\bar{\eta}}\right)_{i-1,j}\right] P_{i-1,j}\Bigg\} \\ & + \frac{1}{2\Delta Y^2}\Bigg\{\left[\left(\frac{\bar{\rho}H^3}{\bar{\eta}}\right)_{i,j+1} + \left(\frac{\bar{\rho}H^3}{\bar{\eta}}\right)_{i,j}\right] P_{i,j+1} \\ & - \left[\left(\frac{\bar{\rho}H^3}{\bar{\eta}}\right)_{i,j+1} + 2\left(\frac{\bar{\rho}H^3}{\bar{\eta}}\right)_{i,j} + \left(\frac{\bar{\rho}H^3}{\bar{\eta}}\right)_{i,j-1}\right] P_{i,j} \\ & + \left[\left(\frac{\bar{\rho}H^3}{\bar{\eta}}\right)_{i,j} + \left(\frac{\bar{\rho}H^3}{\bar{\eta}}\right)_{i,j-1}\right] P_{i-1,j}\Bigg\} - \psi \\ & \cdot \frac{1}{\Delta X}\left\{(\bar{\rho}H^3U)_{i,j} - (\bar{\rho}H^3U)_{i-1,j}\right\} \end{aligned} \tag{11}$$

2.3 Energy Equation and Temperature Profile of Lubricant

The other fundamental equation required is the energy equation as shown in Equation (12). This equation presented is in 2-dimensional form and it is derived for Newtonion fluid.

$$u_{av} T\gamma \frac{\partial p}{\partial x} + \eta\left(\frac{\partial u}{\partial z}\right)^2 = \rho u c_p \frac{\partial T}{\partial x} - k_t \frac{\partial^2 T}{\partial z^2} \tag{12}$$

In dealing with elastohydrodynamic lubricated contacts, the viscous heating and conduction cooling terms are considered more important because of the occurrence of thin films. Therefore, Equation (12) can be further simplified into Equation 13 as shown below [14]:

$$u_{av} T\gamma \frac{\partial p}{\partial x} + \eta\left(\frac{\partial u}{\partial z}\right)^2 = -k_t \frac{\partial^2 T}{\partial z^2} \tag{13}$$

A simplified analytical solution for Equation (13) in solving the temperature profile in the lubricant can then be expressed as follow [3,4]:

$$\Delta T = \left\{\frac{u_{av} T\gamma hp + 2a\bar{\eta}^2/h}{\frac{ak_c}{h} - u_{av}\gamma hp}\right\} \tag{14}$$

2.4 Film Thickness of Lubricant

Under elastohydrodynamic lubrication, there is a certain degree of deformation of the journal bearing. Therefore, the fluid film equation has to be modified and the term deflection, $\boldsymbol{\delta_{k,l}}$ should be considered, which forms [15]:

$$h_{i,j} = C\left(1 - \varepsilon_x \cos\theta_i - \varepsilon_y \sin\theta_i\right) + \delta_{k,l} \tag{15}$$

2.5 Lubricant Rheology

Both density and viscosity of the lubricant are taken to vary with both pressure and temperature in this study. The pressure-temperature-density relationship is shown in Equation (16) [3]:

$$\bar{\rho}_{i,j} = \rho_o \left(1 + \frac{0.6 \cdot 10^{-9} \cdot P}{1 + 1.7 \cdot 10^{-9} \cdot P}\right)(1 - \gamma \Delta T) \tag{16}$$

The effective viscosity of the lubricant under the influence of both temperature and pressure is given as in Equation (17) [3]:

$$\bar{\eta}_{i,j} = \eta_o e^{[\ln \eta_0 + 9.67]\left[-1 + \left(1 + 5.1\times10^{-9}P\right)^Z \times \left(\frac{T-138}{T_o-138}\right)^{-S_o}\right]} \tag{17}$$

where $Z = \frac{\alpha_o}{5.1\times10^{-9}[\ln \eta_0 + 9.67]}$ and $S_o = \frac{\beta_o (T_o - 138)}{\ln \eta_0 + 9.67}$.

2.6 Loading Components in Journal Bearing

In general, the load acting on the journal bearing can be classified into two directions, which are *x*-direction and *y*-direction. A positive load acting in *x*-direction is set as in horizontal and acting to the left. Whilst the positive load acting in *y*-direction is set as in vertical and acting downwards.The load in both directions can be calculated through Equations 18 and 19 respectively [16].

$$W_x = \int_{-\pi}^{\pi} \int_{0}^{L} P_{i,j} \cdot cos\theta_i \cdot R d\theta dy$$

$$W_x = \sum_{i=1}^{M-1} \sum_{j=1}^{N-1} P_{i,j} \cdot cos\theta_i \cdot dxdy \tag{18}$$

$$W_y = \int_{-\pi}^{\pi} \int_{0}^{L} P_{i,j} \cdot sin\theta_i \cdot R d\theta dy$$

$$W_x = \sum_{i=1}^{M-1} \sum_{j=1}^{N-1} P_{i,j} \cdot sin\theta_i \cdot dxdy \tag{19}$$

Therefore, the resultant load for both *x* and *y* component loadings is:

$$W_{resultant} = \sqrt{W_x^2 + W_y^2} \tag{20}$$

2.7 Flow chart for the numerical solution

Figure 1 gives the flow chart of the proposed numerical solution in solving the Reynolds equation. It is to note that the iterative solution is programmed using C-language.

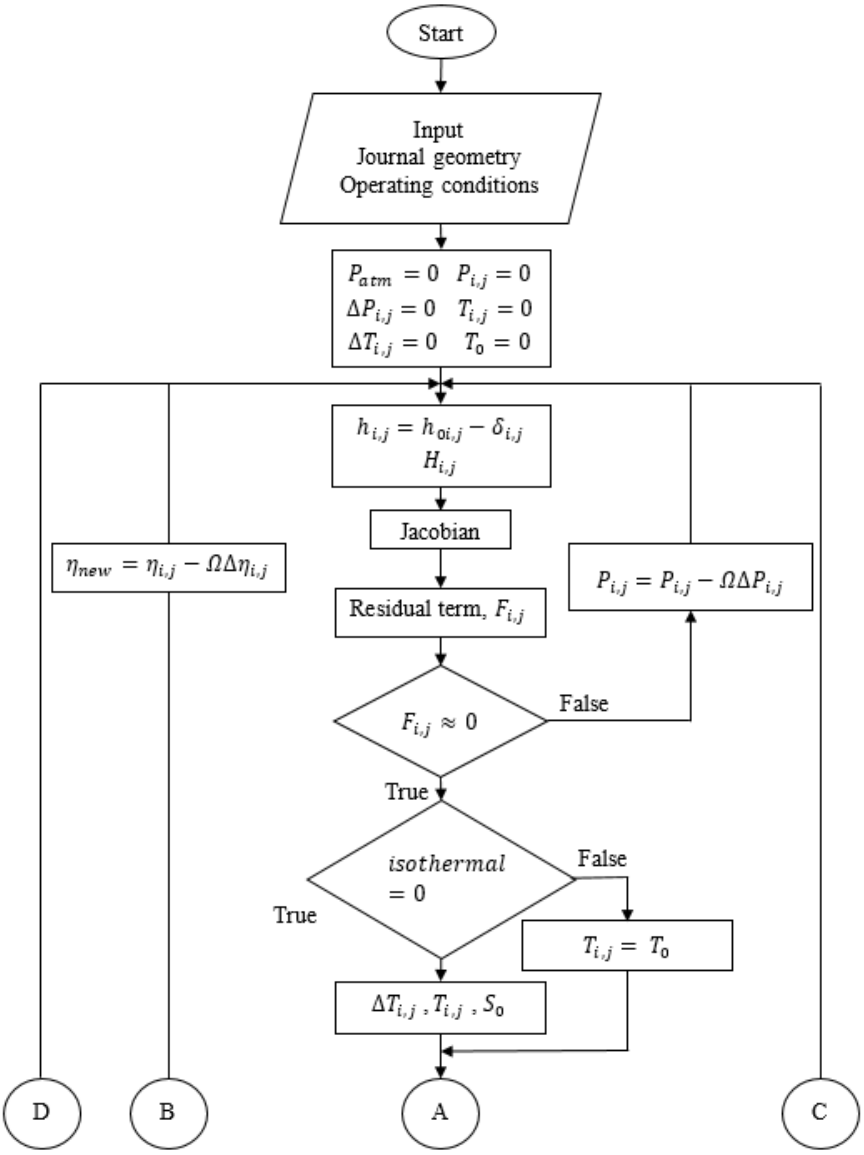

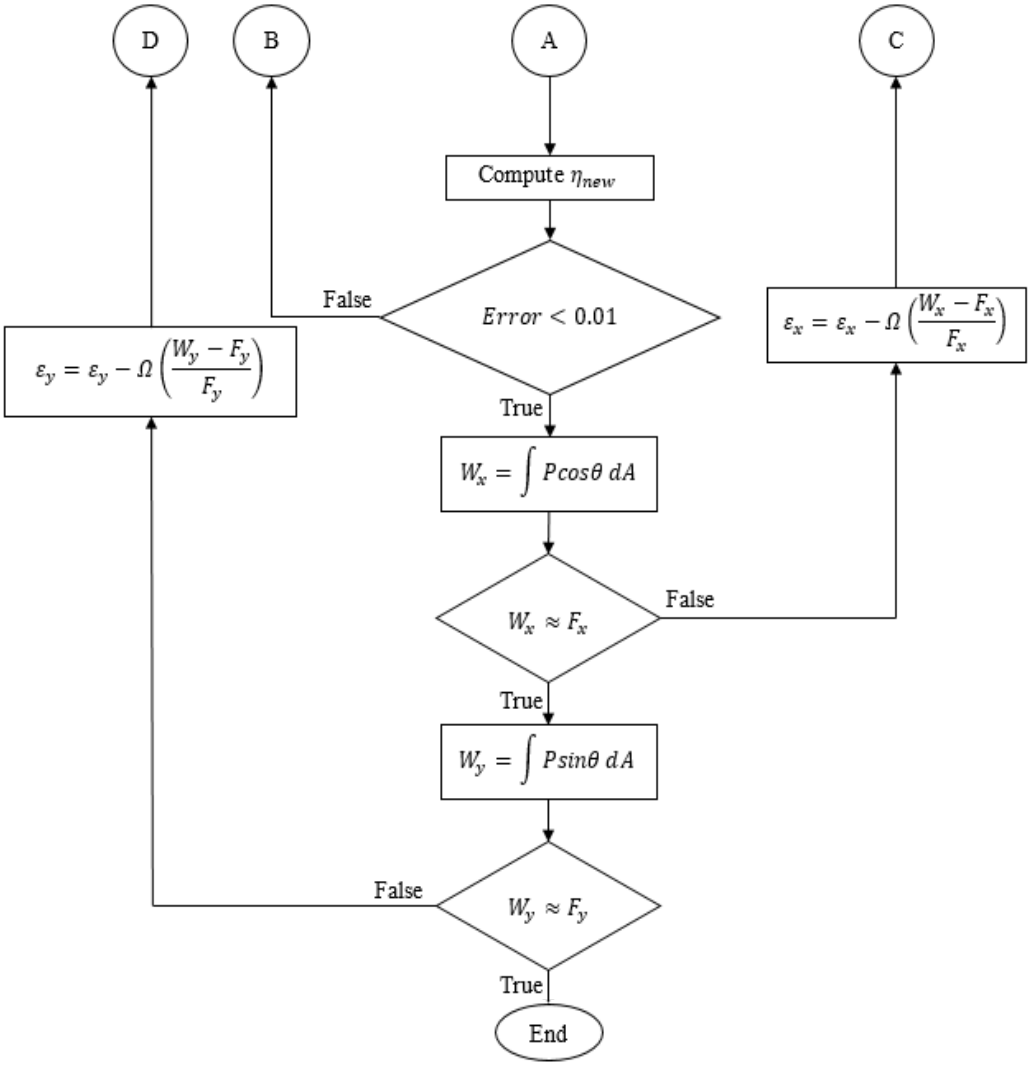

Figure 2: Flow chart for the proposed numerical solution

3.0 RESULTS AND DISCUSSION

Referring to Figure 3,the contact pressure and film profile at both locations exhibit a similar trend, where the contact pressure and film thickness increase with higher lubricant viscosity. When the viscosity of a lubricant is increased, it results in a greater pressure generated as more work is required to slow down the fluid from being entrained into the inlet region. Interestingly, such an action also leads to the formation of a larger film thickness, giving rise to a larger load carrying capacity. It is illustrated in Figure 1(a) that location B portrays a higher velocity than in location A. The higher velocity is demonstrated to generate a larger pressure since it has to slow down the lubricant at a faster rate, hence, resulting in the simulated larger film thickness.

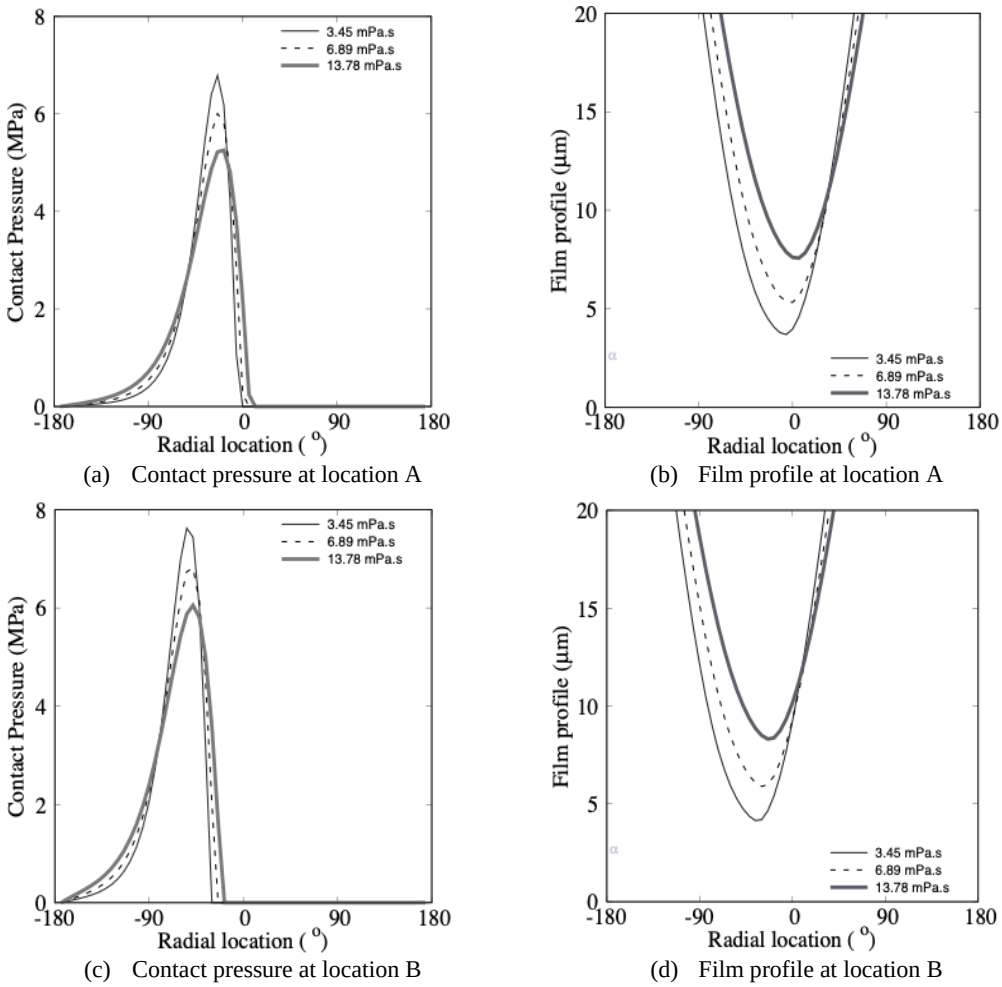

Figure 3: Central cross-section of contact pressure and film profile for piston connecting-rod big end journal bearing with varying lubricant dynamic viscosity (locations A and B given in Figure 1)

It is demonstrated in Figure 1(b) that the applied normal load at location D is higher as compared to that of location C. It is noticed in Figure 4 that the contact pressure at location D is higher due to the difference in the normal applied load. When the load is higher, a higher pressure is developed in the lubrication wedge to lift up the journal bearing as an act of balancing the normal applied load. The lubricant film thickness is shown to broaden when the normal applied load increases due to the higher combustion pressure occurring at location D. The higher normal applied load is also shown to subject the journal bearing to significant elastic deformation. For the simulated journal bearing, the influence of load on the film thickness is considerably small because film thickness is more sensitive to the change in lubricant properties, velocity of moving surfaces and radius of curvature. However, on the other hand, the normal applied load could influence the shape of the film profile when elastic deformation becomes apparent.

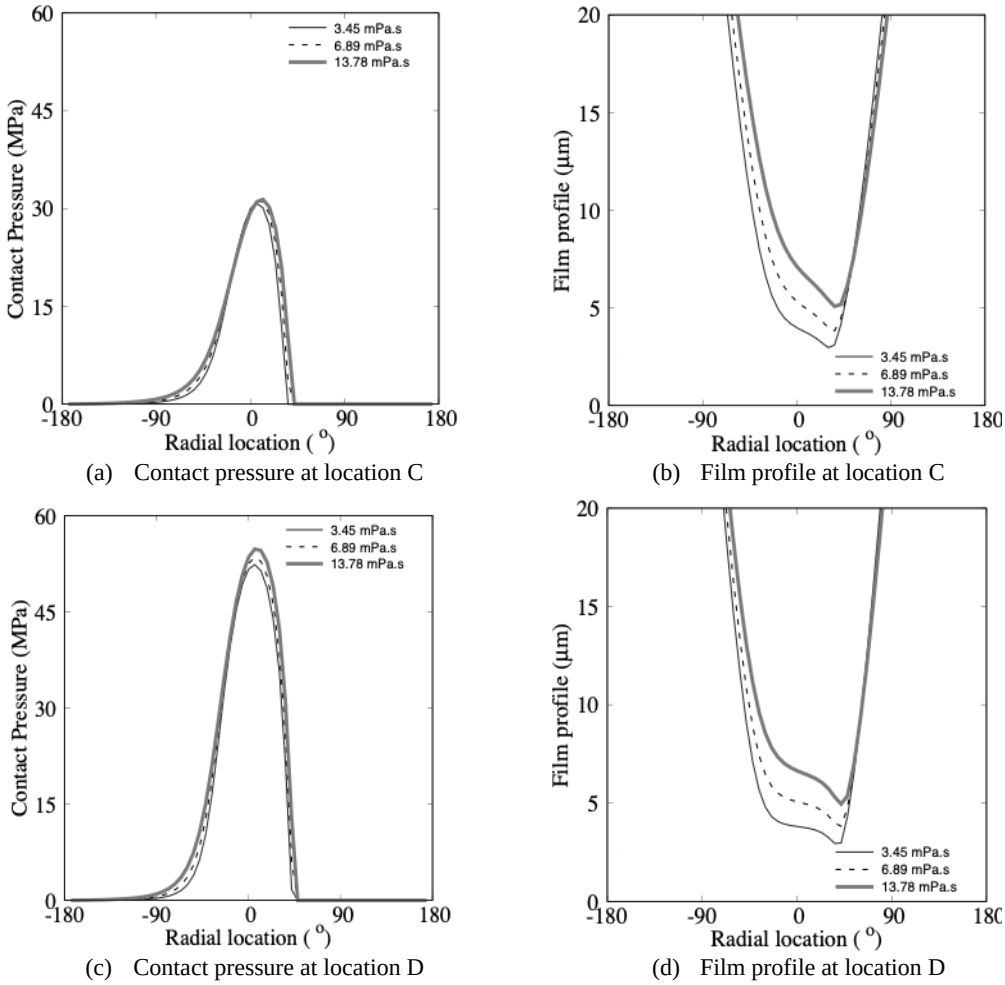

(a) Contact pressure at location C (b) Film profile at location C

(c) Contact pressure at location D (d) Film profile at location D

Figure 4: Central cross-section of contact pressure and film profile for piston connecting-rod big end journal bearing with varying lubricant dynamic viscosity (locations C and D given in Figure 4.1)

Different cases are conducted on both isothermal and thermal analysis for four different operating conditions as highlighted in Figure 1. As it can be observed in Figure 5, the minimum film thickness at location B is slightly higher than that at location A because at a lower velocity, the journal tends to weigh downwards due to its weight and presses against the lubricant film, resulting in smaller film thickness. Whilst at a higher velocity, the journal tends to float around, producing a lift-off effect, which results in a larger film thickness.In both isothermal and thermal analysis, a distinct deviation occurs at a higher velocity. The minimum film thickness when thermal effects are taken into consideration is smaller due to the significant temperature rise by viscous heating, which lowers the lubricant viscosity.

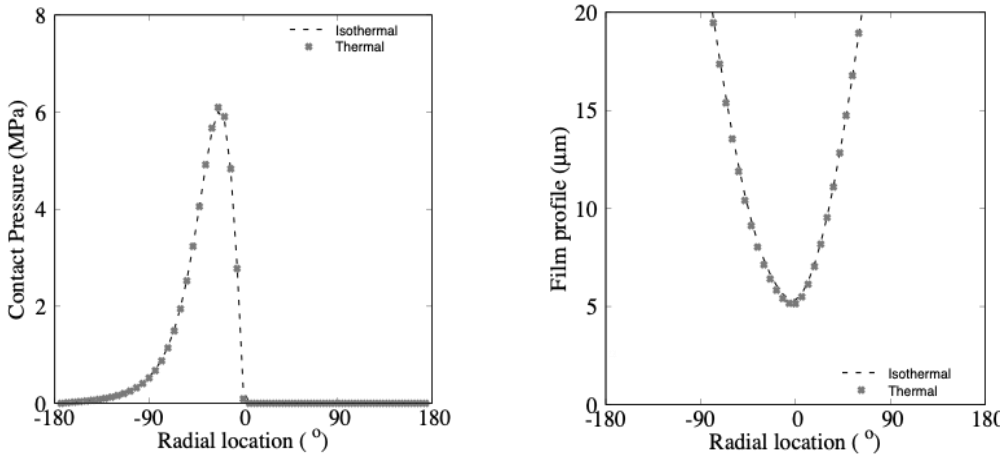

(a) Contact pressure at location A (b) Film profile at location A

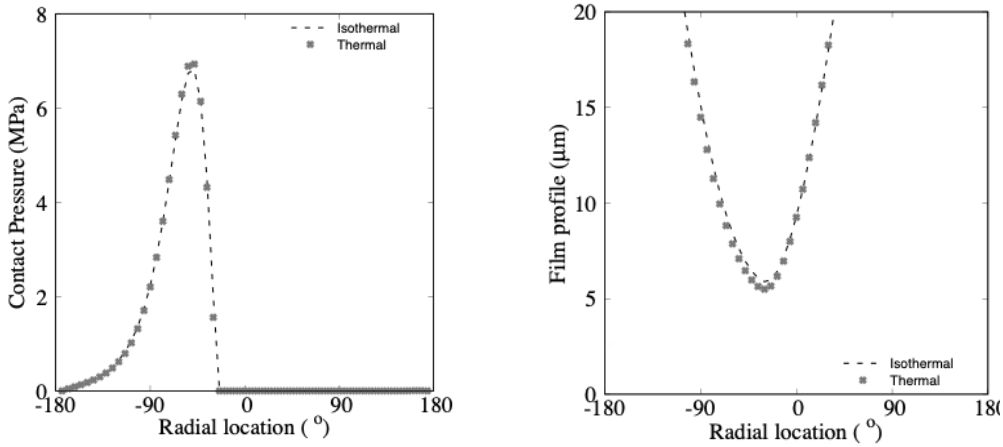

(c) Contact pressure at location B (d) Film profile at location B

Figure 5: Central cross-section of contact pressure and film profile for piston connecting-rod big end journal bearing at different operating conditions (locations A and B given in Figure 4.1)

As load is increased, the film stiffness increases, which leads to the rising of the temperature. The rise of temperature for higher load exceeds the lower load temperature rise, which could be reason for the deviation shown in the film profile at location D compared to location C (see Figure 6). It is to note that no deviation in terms of contact pressure is observed. This is because even though the thermal assumptions are different, the normal applied normal load remains constant the same at these locations. It is instead reflected that to achieve the same amount of load carrying capacity (contact pressure), a smaller film thickness is required for the contact with lower lubricant viscosity, such as the one experienced when temperature effect is being accounted for the sliding contact.

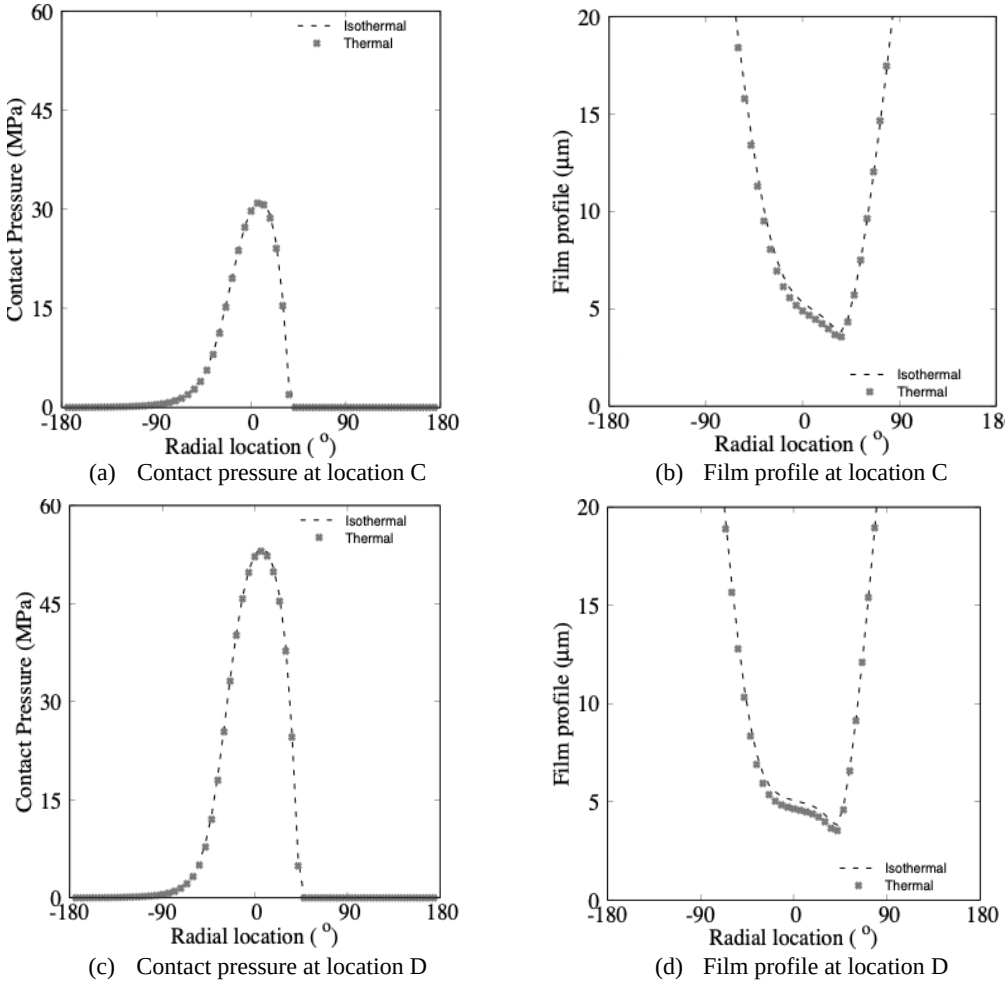

(a) Contact pressure at location C (b) Film profile at location C

(c) Contact pressure at location D (d) Film profile at location D

Figure 6: Central cross-section of contact pressure and film profile for piston connecting-rod big end journal bearing at different operating conditions (locations C and D given in Figure 4.1)

In Figure 7, it can be observed that the temperature profile increases with engine speed, along with the increment in the inertia load, dynamic loading and the velocity of journal bearing. Under the circumstance of increased inertia load and dynamic loading, lubricant film thickness tends to decrease. With the decreased film thickness and increased velocity of journal bearing, shear stress increases, resulting in the rising of the temperature of bearing. Similarly, in Figure 8, the temperature profile increases with the applied normal load. Increased applied normal load leads to higher dynamic loading, higher stiffness and lower minimum film thickness, which promote the increasing of heat generation with the temperature of the solid surfaces tend to rise at the same time.

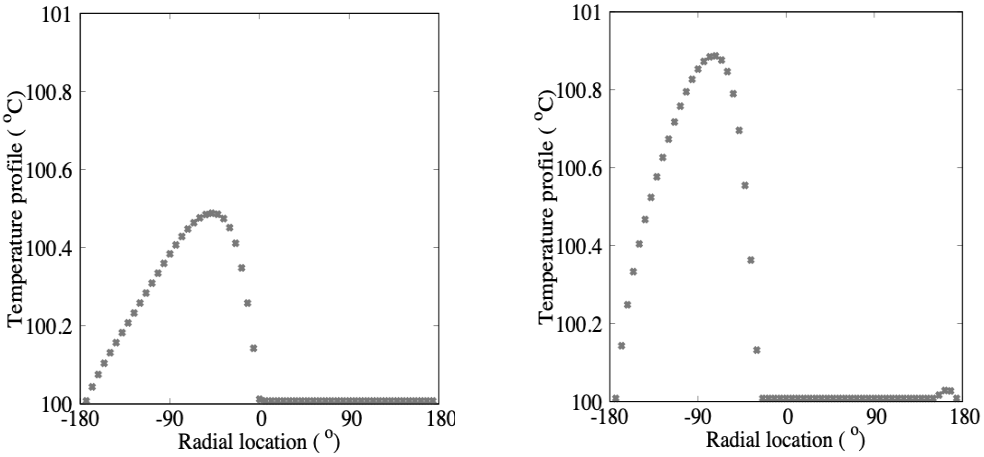

(a) Location A (b) Location B

Figure 7: Central cross-section of temperature profile for piston connecting-rod big end journal bearing at different operating conditions (locations A and B given in Figure 4.1)

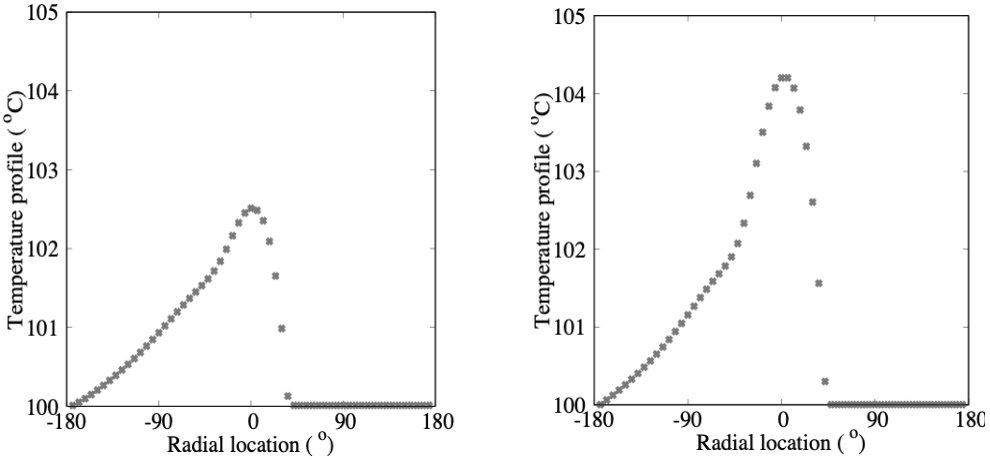

(a) Location C (b) Location D

Figure 8: Central cross-section of temperature profile for piston connecting-rod big end journal bearing at different operating conditions (locations C and D given in Figure 4.1)

Figure 9 illustrates a comparison of the literature data obtained from reference [11,12] with the simulated results. It is observed that the trend for both isothermal and thermal analysis has similarities with the overall shape of the extracted literature data. However, this comparison shows obvious deviation starting from crank angle around 0° and onwards. The predictions of maximum contact pressure can be observed to be lower by as much as 42% when compared with the literature data. This is believed to be the result of the elimination of squeeze film effect in this study. Squeeze film occurs due to relative normal motion, where two surfaces move towards each other in the normal direction, providing a cushioning effect in the bearings. This phenomenon generates a positive pressure, which supports a load. Neglecting this effect, such as the one adopted in this study, could have led to the lower generated contact pressure.

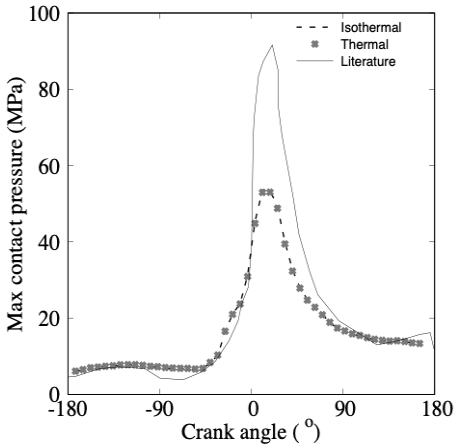

Figure 9: Maximum contact pressure of the investigated piston connecting-rod big end journal bearing at different crank angles (literature data extracted from reference [13])

In the present study, the critically loaded region for the piston connecting-rod big end journal bearing along the engine cycle is selected for investigation as given in Figure 1. The minimum film thickness of the simulated film profile is then determined at each crank angle as given in Figure 10 in comparison with the data given in literature [11,12]. Because of the strong temperature-dependence of viscosity, any rise in temperature could reduce the lubricant viscosity. Therefore, it can be observed that trend when thermal effects are taken into consideration is not aligned with the isothermal analysis. Based on Figure 10, the minimum film thickness predicted is within a similar range as given in literature. However, the predictions of the minimum film thickness could only show reasonable agreement with the literature data at an offset trend (estimated to be approximately 40° offset to the left), especially at the power stroke region (highly pressurized region). This could be attributed to the assumption of the present study, where no squeeze film effect is being considered. The impact coming from the squeeze film, which is as a function of the sliding velocity and normal applied load, could have delayed the drop in the film thickness when the contact is subjected to higher normal applied load.

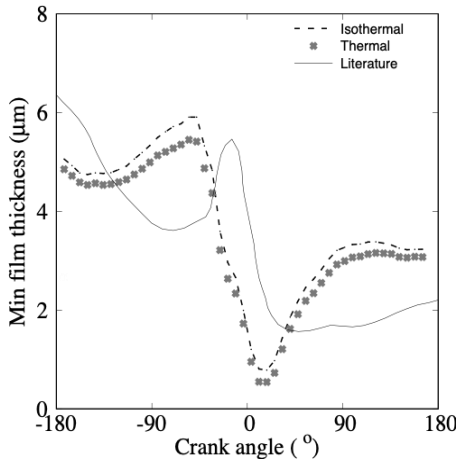

Figure 10: Minimum film thickness of the investigated piston connecting-rod big end journal bearing at different crank angles (literature data extracted from reference [13])

4.0 CONCLUSION

Overall, by considering isothermal condition and varying the lubricant dynamic viscosity, greater hydrodynamic pressure is generated, and larger film thickness is formed as the viscosity increases. Similarly, an increase in the velocity or applied normal load results in higher contact pressure and larger film profile. When thermal effects are taken into consideration, the presence of viscous heating during the engine operation leads to a significant temperature rise, which directly lowers

the lubricant viscosity. As a response, the film thickness reduces. In addition, the temperature profile increases with engine speed as well as the normal applied load. Under this scenario, the dynamic loading in the piston connecting-rod big end journal bearing increases, which results in the reduction of film thickness, higher heat generation and the rising of the temperature. Generally, small deviations have been observed in the contact pressure and film thickness profile when thermal effects are considered in the analysis. The deviations could be considered as small and trivial, but thermal effect towards the lubricant would become critical and ought to be considered for a better prediction of friction and power losses. On the other hand, when comparing the predicted minimum film thickness across a single engine cycle operation, it is determined that the present mathematical model is capable of predicting film thickness in a similar range as reported in literature under similar operating conditions. However, at the highly pressurized region, the simulated minimum film thickness possesses a similar trend but at an offset behavior. This is believed to be as a result of the assumption taken in the present study, which is to exclude the effect of squeeze film.

ACKNOWLEDGEMENTS

First and foremost, I would like to express my sincere gratitude to my supervisor, Dr William Chong Woei Fong for his continuous invaluable guidance, suggestions and comments throughout the project. I would specially thank him for constantly motivating me to stay positive and work harder. Without his persistent help, I would not have successfully completed this thesis. On the other hand, I am indebted to UniversitiTeknologi Malaysia (UTM) for providing me with all the facilities and relevant literature resources from the library. My appreciation also extends to my friends, who have provided assistance and opinions throughout the course of the project.

REFERENCES

[1] Holmberg, K., Andersson, P. and Erdemir, A., 2012. Global energy consumption due to friction in passenger cars. *Tribology international*, *47*, pp.221-234.

[2] Chong, W.W.F., Ng, J.H., Rajoo, S. and Chong, C.T., 2018. Passenger transportation sector gasoline consumption due to friction in Southeast Asian countries. *Energy conversion and management*, *158*, pp.346-358. [3]

[3] Karthikeyan, B.K., Teodorescu, M., Rahnejat, H. and Rothberg, S.J., 2010. Thermoelastohydrodynamics of grease-lubricated concentrated point contacts. *Proceedings of the Institution of Mechanical Engineers, Part C: Journal of Mechanical Engineering Science*, *224*(3), pp.683-695.

[4] Chong, W.W.F., Teodorescu, M. and Rahnejat, H., 2014. Mixed thermo-elastohydrodynamic cam–tappet power loss in low-speed emission cycles. *International Journal of Engine Research*, *15*(2), pp.153-164.

[5] Kim, B.J. and Kim, K.W., 2001. Thermo-elastohydrodynamic analysis of connecting rod bearing in internal combustion engine. *J. Trib.*, *123*(3), pp.444-454.

[6] El-Butch, A.M., 2002. Transient Thermo ElastoHydrodynamic Lubrication of Connecting Rod Big-End Bearings. *SAE Transactions*, pp.760-766.

[7] Cheng, H.S. and Sternlicht, B., 1965. A numerical solution for the pressure, temperature, and film thickness between two infinitely long, lubricated rolling and sliding cylinders, under heavy loads.

[8] Kim, H.J., Ehret, P., Dowson, D. and Taylor, C.M., 2001. Thermal elastohydrodynamic analysis of circular contacts part 1: Newtonian model. *Proceedings of the Institution of Mechanical Engineers, Part J: Journal of Engineering Tribology*, *215*(4), pp.339-352.

[9] Gao, G., Yin, Z., Jiang, D. and Zhang, X., 2014. Numerical analysis of plain journal bearing under hydrodynamic lubrication by water. *Tribology International*, *75*, pp.31-38.

[10] Zhang, H., Zhu, C. and Yang, Q., 2008, October. Approximate numerical solution of hydrodynamic gas journal bearings. In *International Conference on Intelligent Robotics and Applications* (pp. 260-268). Springer, Berlin, Heidelberg.

[11] Paranjpe, R.S., Tseregounis, S.I. and Viola, M.B., 2000. Comparison between theoretical calculations and oil film thickness measurements using the total capacitance method for crankshaft bearings in a firing engine. *Tribology transactions*, *43*(3), pp.345-356.

[12] Chai, B.Y.B. and Chong, W.W.F., 2019. Predicting frictional losses generated by piston connecting-rod big end journal bearing for an internal combustion engine. *Journal of Transport System Engineering*, *6*(1).

[13] Chong, W.W.F., Hamdan, S.H., Wong, K.J. and Yusup, S., 2019. Modelling Transitions in Regimes of Lubrication for Rough Surface Contact. *Lubricants*, *7*(9), p.77.

[14] Rahnejat, H. and Gohar, R., 2018. *Fundamentals of tribology*. World Scientific.

[15] Wang, D., Keith, T.G., Yang, Q. and Kumar, V., 2004. Lubrication analysis of a connecting-rod bearing in a high-speed engine. Part I: rod and bearing deformation. *Tribology transactions*, *47*(2), pp.280-289.

[16] Wang, D., Keith, T.G., Yang, Q. and Kumar, V., 2004. Lubrication analysis of a connecting-rod bearing in a high-speed engine. Part II: lubrication performance evaluation for non-circular bearings. *Tribology transactions*, *47*(2), pp.290-298.